BNL-107823-2015-JA

Quantitative characterization of arc discharge as vacuum interface

S. Huang[1], K. Zhu[1], Y. R. Lu[1], S. Z. Wang[1], A. Hershcovitch[2], L. Yang[3], and X. Y. Zhang[3]

[1]State Key Laboratory of Nuclear Physics and Technology,
Peking University, Beijing 100871, China
[2]Brookhaven National Laboratory, Upton, NY 11973 USA
[3]Institute of Modern Physics, Chinese Academy of Sciences,
Lanzhou 730000, China

Submitted to Physics of Plasmas

December 2014

Collider-Accelerator Department

Brookhaven National Laboratory

U.S. Department of Energy
Office of Science, Office of Nuclear Physics

Notice: This manuscript has been co-authored by employees of Brookhaven Science Associates, LLC under Contract No. DE-AC02-98CH10886/DE-SC0012704 with the U.S. Department of Energy. The publisher by accepting the manuscript for publication acknowledges that the United States Government retains a non-exclusive, paid-up, irrevocable, world-wide license to publish or reproduce the published form of this manuscript, or allow others to do so, for United States Government purposes.

DISCLAIMER

This report was prepared as an account of work sponsored by an agency of the United States Government. Neither the United States Government nor any agency thereof, nor any of their employees, nor any of their contractors, subcontractors, or their employees, makes any warranty, express or implied, or assumes any legal liability or responsibility for the accuracy, completeness, or any third party's use or the results of such use of any information, apparatus, product, or process disclosed, or represents that its use would not infringe privately owned rights. Reference herein to any specific commercial product, process, or service by trade name, trademark, manufacturer, or otherwise, does not necessarily constitute or imply its endorsement, recommendation, or favoring by the United States Government or any agency thereof or its contractors or subcontractors. The views and opinions of authors expressed herein do not necessarily state or reflect those of the United States Government or any agency thereof.

Quantitative Characterization of Arc Discharge as Vacuum Interface

S. Huang,[1] K. Zhu,[1,a)] Y. R. Lu,[1] S. Z. Wang,[1] A. Hershcovitch,[2] L. Yang,[3] and X. Y. Zhang[3]
[1]State Key Laboratory of Nuclear Physics and Technology, Peking University, Beijing 100871, China
[2]Brookhaven National Laboratory, Upton, New York 11973, USA
[3]Institute of Modern Physics, Chinese Academy of Sciences, Lanzhou 730000, China

Abstract:

An arc of certain parameters can separate between vacuum and atmosphere or between vacua regions of different pressures, thus function as a Plasma Window. A Plasma Window, operating in argon, with discharge channel diameters of 3mm and 6mm and lengths between 30mm and 60mm was experimentally investigated for empirical characterization. Electron temperature of the plasma channel, which was measured spectroscopically, varies in the range of 7000K to 15000K, increasing with increasing current and decreasing gas flow rate. That plasma window has a slightly positive I-V characteristics over the whole range of investigated current 30A-70A. Measuremnts of pressure separation capability, which is determined by input current, gas flow rate, discharge channel diameter and length, can be well explained by viscosity effect and "thermal-block" effect. The experimental results of global parameter including temperature, gas flow rate and voltage have a good agreement with the simulation results calculated by an axis-symmetry Fluent-based magneto-hydrodynamic model.

[a)]zhukun@pku.edu.cn

1. Introduction

Windowless vacuum sealing technique can separate vacuum from high pressure targets or atmosphere without solid window. As a result, it can reduce most of the interactions between injected particles and materials comparing with foil windows. It has been widely researched and

designed in low-energy nuclear experiments and in some experiments with high-intensity high-energy particle beams which can destroy foils and other windows in a short time. It is also desired in experiments, which require injecting high purity mono-energetic beams and, in intense mono-energetic neutron sources[1, 2] for example. Increasing sealing pressure capability and decreasing gas flow rate are the research and main goals of windowless vacuum separation techniques.

This technique was first realized by injecting supersonic gas jets through tubes into a vacuum chamber which are evacuated by differential pumping systems[3-7]. However, its sealing pressure is limited (below 10kPa) and the gas flow consumption is rather high. Bonin and MacIlrath [8] improved this method by applying a rotating disk valve to the differential pumping system. The sealing pressure can be increased by an order of magnitude (up to 1 atmosphere) comparing with previous differentially pumped values. However, this valve system requires injection of pulse beam at low duty factor, and synchronized frequency control with high precision.

The plasma window, which invented by Ady Hershcovitch[9] in 1995, is a novel apparatus for windowless vacuum sealing solution. It utilizes cascaded an arc discharge[10] to form a high temperature plasma column in the arc channel. With such a high temperature and pressure plasma, a vacuum-high pressure interface can be established and maintained between the two ends of the plasma window. It was first demonstrated by being used to transmit, from vacuum through a plasma window to atmosphere (or high pressure targets electron beams[11, 12], a 2MeV proton beam[13] and synchrotron radiation[14]. Furthermore, plasma windows were explored to function as a deuteron gas target[2] and charge stripper gas target by Kuboki[15]. A numerical 2D FLUENT-based magneto-hydrodynamic model in reference 16 has been developed, through which the validation for the sealing ability of plasma window was verified. However sealing characteristics and plasma properties of these plasma windows were rarely researched[17]. W A J Vijers has done a lot of experimental and theoretical characterization work with a similar device, which functioned as a plasma source[18, 19].

In this paper, we will first present a typical design of the plasma window in section 2. Spectroscopic plasma diagnostics methods will be illustrated. In section 3, experimental data will

be shown and the influence of plasma channel spatial parameters (discharge diameter and length), and the operating conditions (gas flow and arc current) on sealing pressure capability, electron temperature and current voltage (I-V) characteristics will be discussed. In section 4, the vacuum separation characteristics are first explained by viscosity effect and "thermal blocking" effect qualitatively. Furthermore, experimental and detailed simulation results of MHD model are compared and discussed. In section 5, general conclusions are presented.

2. Experimental Setup and Diagnostics

A. Plasma window

A schematic of the plasma window is shown in Fig. 1. It is mainly composed of cascade of 9mm thick copper plates which are pressed together by a cathode housing structure and an anode plate. Electrical insulation and vacuum sealing, among the plates cathode housing and anode plate, are accomplished by 1mm thick boron nitride spacer plates inside O-rings, mechanically stabilized by PEEK material washers outside the O-rings. The total thickness and bore diameter of cascaded plates (and boron nitride spacers) determine the length and diameter of plasma window channel respectively. Two types (3mm and 6mm) of copper plate diameter were used in the present experiments. Three cathodes are inserted at an angle of 45° into cathode chamber. Cathodes and anode are connected to a constant-current power supply which can deliver current up to 80A. The power supply is integrated with a high voltage AC triggering system that can provide an alternating current output voltage of more than 6000V to ignite arc easily. Once the arc is ignited the power supply can be changed to DC mode alternatively. Circuit with LC filters plus high-power resistors implanted in power supply can stabilize the arc.

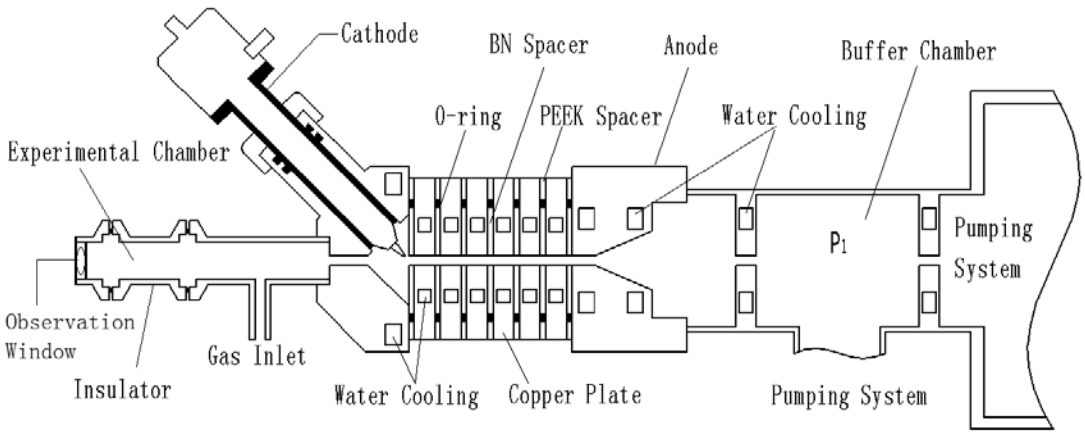

Figure 1: Schematic figure of plasma window

Argon gas is feed to plasma window (PW) through gas inlet tube and the gas flow rate is monitored by Seven Star D07-9E gas flowmeter. Pressure in the experimental chamber (Inlet Pressure), which ranges from 10-100kPa during operation, is depended on channel diameter, length, gas flow rate and discharge current. It is measured with a DL-04 Varistor pressure gauge. The low pressure end of the PW is connected to a buffer chamber which is pumped by a differential pump system with combination of roots pump and claw-type pump (effective pumping rate of ~15L/s). The pressure in the buffer chamber varies from 10Pa to 200Pa, measured by a DL-03 thermocouple gauge.

B. Plasma Spectroscopy setup and methodology

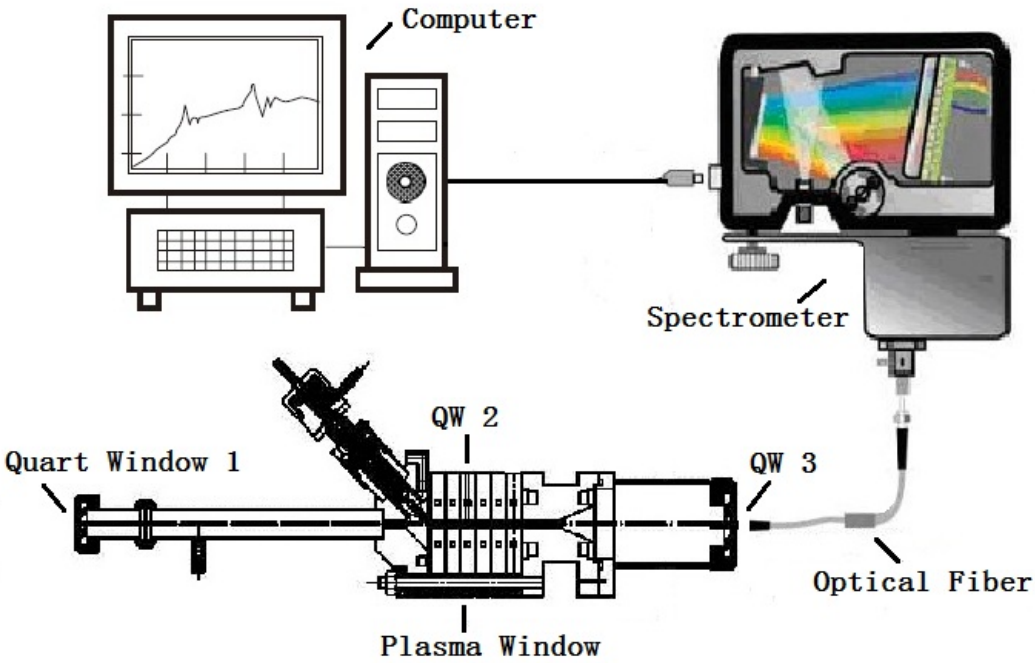

Figure 2: Schematic diagram of the spectroscopy setup

A spectroscopy setup (please see Fig. 2) consists of a spectrometer (Horiba iHR 550) along with a CCD camera (Synapse), power supplies, and a computer for running the spectroscopy program (SynerJY). Spectrum signal, which passes through quartz windows (QW), is be collected by optical fiber connected to spectrometer. The spectrometer has three different gratings (300gr/mm, 1200gr/mm and 2400gr/mm) to satisfy the requirements of spectral coverage and resolution.

Different spectral lines are scanned from 410nm to 550 nm, and spectral intensity as a function of wavelength is recorded in the program. Intensity values at the same point are obtained by average of 10 times measurements to minimize the effect of intensity fluctuation. The electron excitation temperature of arc plasma along the line of sight can be determined by atomic Boltzmann plot method[20] from the following equation:

$$\log(I\lambda / g_k A_k) = C - E_k / \mathrm{k}T$$

where I is measured spectrum intensity and λ is the wavelength of the line. A_k, E_k and g_k are transition probability, excitation energy and statistical weight of atomic state k, respectively, values of which can be found in literature[20]. A plot between $\log(I\lambda / g_k A_k)$ and E_k yields a straight line by linear fitting method. The inverse of line slop gives the electron temperature of the plasma arc by assuming that the population of the emitting levels follows the Boltzmann's distribution.

The Stark broadening of a certain spectral line emitted from plasma allows the determination of the electron density. The broadening half-width($\Delta\lambda_{1/2}$) of spectral line is proportional to electron density[21] :

$$\Delta\lambda_{1/2} = 2w\frac{N_e}{10^{16}} + 3.5\alpha(1-\frac{3}{4}N_D{}^{-1/3})w\frac{N_e}{10^{16}} \text{ Å}$$

Where w is the electron impact parameter, α is the ion impact parameter. Usually in order to simplify, a curve-fitted empirical formula is adopted for calculating the electron density N_e (cm^{-3}) using the half-width of argon I line. The formula [22] is given by:

$$\log N_e = 17.432 + 0.662\log\Delta\lambda_{1/2}$$

The argon I line 430nm is often used to calculate the electron density, as it is separated from other lines, which guarantees a good resolution and accuracy.

3. Experimental Results and Discussion

A. Plasma parameters

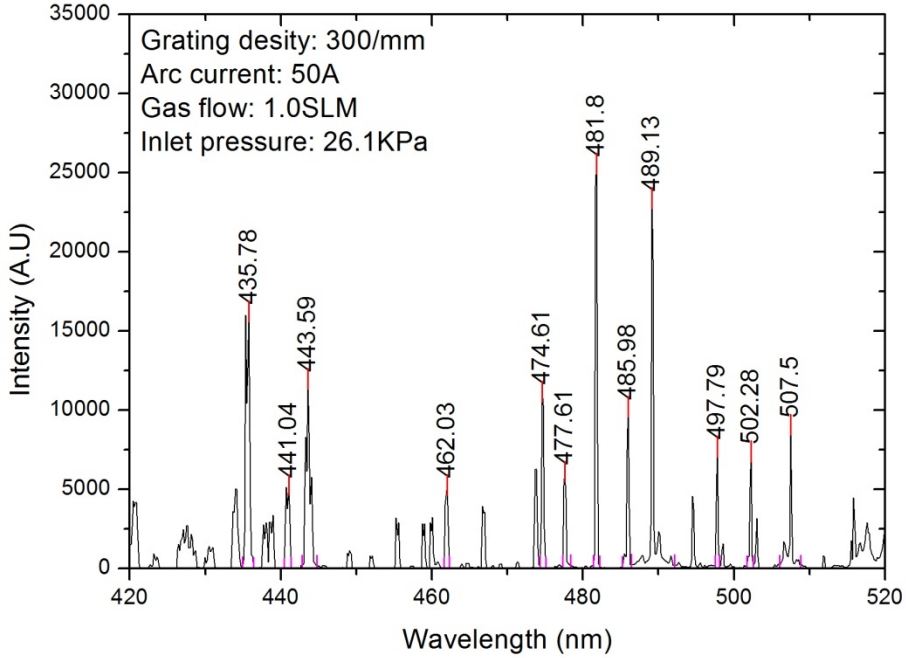

Figure 3: A typical emission spectra of argon lines in the spectral range of 420-520nm for calculation of electron temperature. Channel diameter3mm, channel length 60mm, argon gas flow rate 1SLM, and arc current 50A.

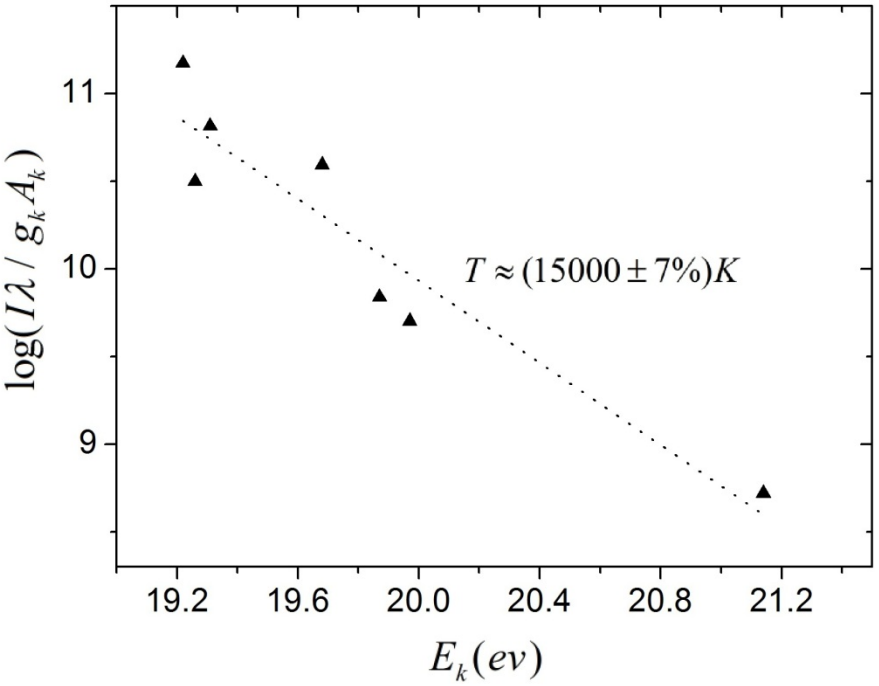

Figure 4: Typical Boltzmann plot for selected Ar emission lines. Argon gas flow rate 1SLM and arc current 50A.

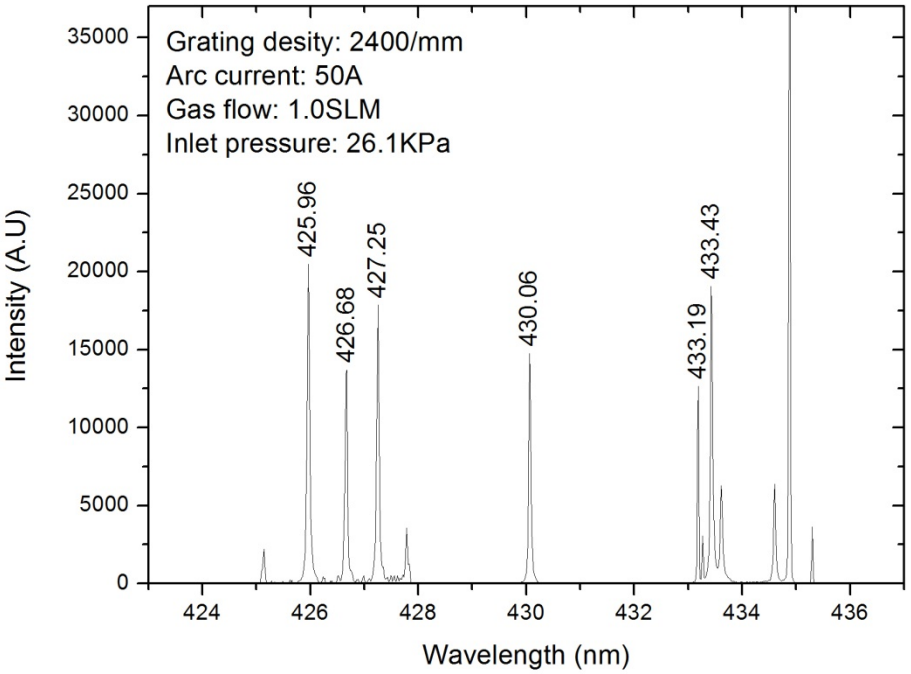

Figure 5: typical emission spectra of argon 430nm line in the spectral range of 424-436nm for calculation of electron density. Channel diameter 3mm, channel length 60mm, argon gas flow

rate 1SLM, and arc current 50A.

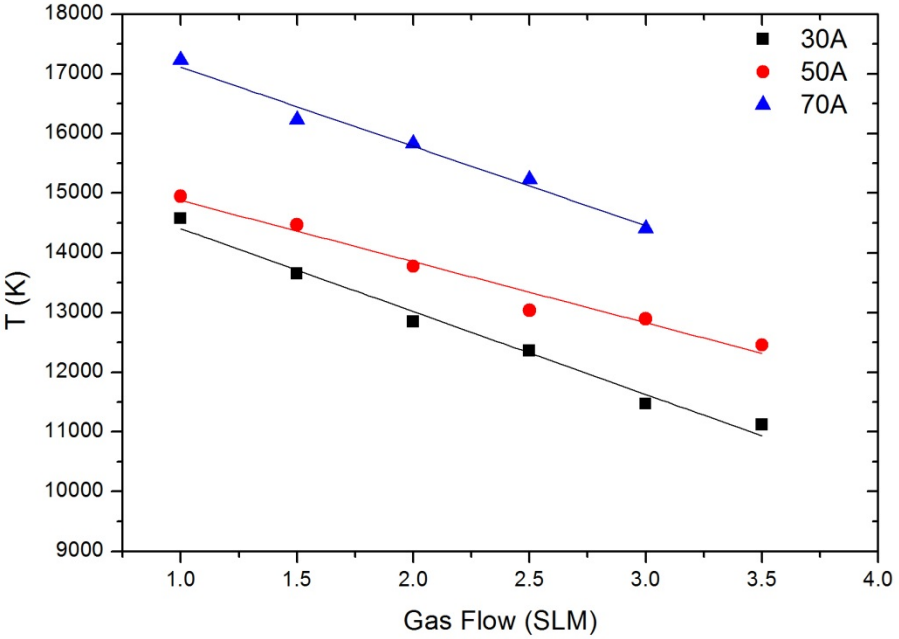

Figure 6: Temperature of argon plasma as a function of gas flow rate for arc currents between 30A and 70A.

A typical spectrum of argon plasma in the spectral range of 400-450nm was shown in figure4 with grating density 300gr/nm. Seven resolved and distinct argon I lines were chosen and corresponding g_k , A_k , E_k were taken from literature. $\log(I\lambda / g_k A_k)$ Vs. E_k were plotted in figure 5, and the slope was obtained from the best linear fitting. The correlation coefficient was more than 0.85 and the relative error of slop was lower than 7% . The electron temperature is calculated out to be about 15000K at gas flow rate of 1SLM and an arc current of 50A. Figure 6 shows a typical spectrum in the range of 422-438nm using grating density 2400/mm. The 430nm line is well separated from others. The electron density is about $3.4\times10^{15}cm^{-3}$. It is known that Ohmic heating is the only source of thermal energy in the plasma, which means that electrons get accelerated in electric field. Meanwhile, part of electron's energy is transferred to heavy particles by elastic and inelastic collisions (i.e. heating and ionization). As electron density increases, both of the average elastic and inelastic collision frequencies will increase too[23]. And that will increase the energy transfer rate from electrons to heavy particles, which will diminish the difference between electron's and heavy particles' temperature as a result. According to theoretical criteria for local thermal equilibrium (Griem 1964[24], Drawin 1969[25]), with typical values for argon plasma at one atmosphere and electron temperature of 10000K, the critical electron density needs to be ranging from $10^{16}cm^{-3}$ to $10^{18}cm^{-3}$. When considering radiation absorption and resonance absorption for lower pressure plasma, the criteria could be decreased. In Kolesnikov[26] and Bourasseau'[27] experimental investigations, results show that local thermodynamic equilibrium (LTE) can be established when electron density is around $5\sim8\times10^{15}cm^{-3}$. Arc plasma inside plasma window is stabilized by the cooled wall, high gradient temperature and velocity distribution leads to non-uniform property. As a result, only

the plasma in the axial region can be close to LTE. The temperature of the gas will be quite lower than the detected electron temperature. A Gleizes has presented the experimental and calculated value of (Te-Th) as a function of electron density for stationary argon arc plasma at atmospheric pressure and electron temperature is estimated to be 1500K higher than that of heavy particles at electron density of $4\times10^{15}cm^{-3}$ [28].

We measured the electron temperature for Φ3mm plasma window at gas flow rates from 1.0 to 4.0 SLM, arc currents of 30, 50, 70A, as shown in figure 7. As it can be seen, the peak temperature ranges from 9000K to 17000K strongly affected by current and argon gas flow rate. The temperature decreases with increasing the gas flow and increases with increasing the arc current, and these trends have a good agreement with W.A.J. Vijers' results[18, 19]. As increasing gas flow rate will lead to increase of inlet pressure. According to Ref. 29, electron temperature will decrease as increasing the pressure in the discharge channel. Therefore, electron temperature will decrease as increasing gas flow rate.

B. I-V Characteristics

Figure 7 shows in detail the results of I-V characteristics for 3mm and 6mm plasma window. The total arc voltage increases slightly as a function of increasing the current from 30A to 70A, which shows cascaded arc of plasma window has a slightly positive I-V characteristics over the whole range of investigated current. This can be ascribed to radiation process, which will increase arc voltage and elevate I-V slope. Especially for low current arc, I-V characteristics become positive[30]. We can find that the voltage increase a little as increasing gas flow. The volt-ampere characteristics for larger diameter 6mm is almost the same with 3mm. The voltage of Φ6mm is almost half of Φ3mm at given current and gas flow. The total voltage of plasma window can be approximately written as $U = IR_{equivalent} = I\dfrac{l}{\pi r^2\sigma(T,P)}$, where r and l are discharge radius and length. The average electric conductivity σ is mainly affected by plasma temperature and pressure, Murphy[31]. From that reference, the average temperature of plasma can be determined by calculating out the average electric conductivity. As the temperature decreases with increase of gas flow rate as shown in figure 6, the electric conductivity will increase a little, which leads to the voltage increase with gas flow rate. For larger diameter plasma window, the average temperature will be much lower at the same current. Consequently, although the cross-section area of Φ6mm aperture is four times of that of the Φ3mm aperture; but, the total votage in the case of the Φ6mm aperture is only twice of that of the Φ3mm aperture as shown in figure 7.

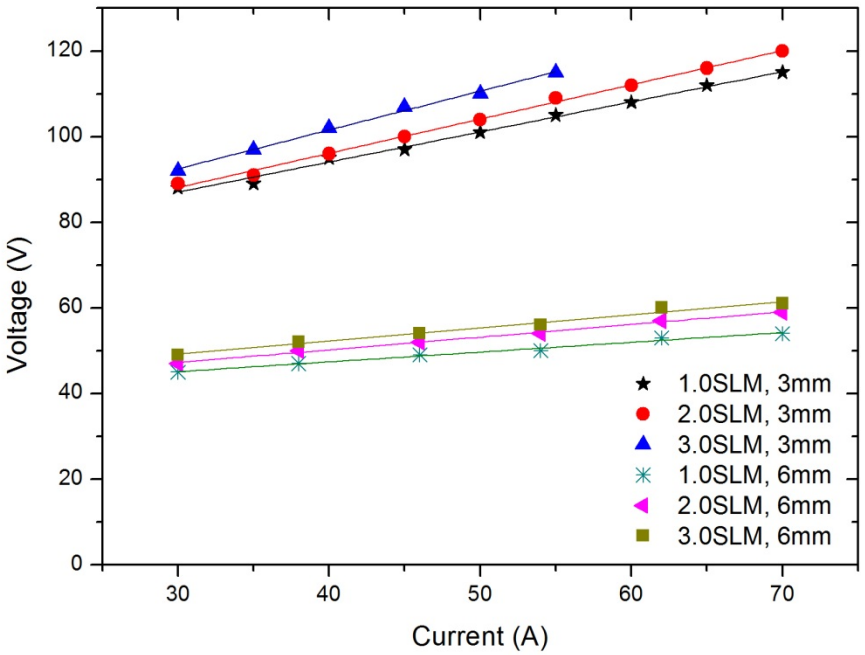

Figure 7: I-V characteristics at argon gas flow rate between 1.0SLM and 3.0SLM for channel diameter 3mm and 6mm.

C. Pressure Measurements

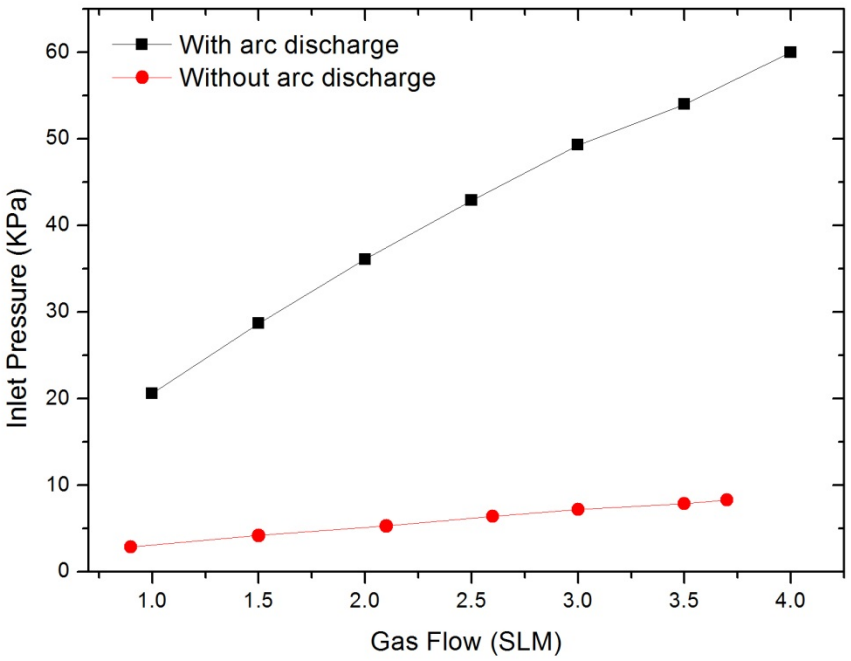

Figure 8: Pressure in the experimental chamber as a function of argon gas flow rate with and without arc discharge. The diameter and length of the plasma channel is 3mm and 60mm respectively, and the discharge current is 50A.

To show sealing effect of plasma window directly, inlet pressure was measured as a function of argon gas flow rate between 0.5 and 4.0SLM for plasma window on and off. The diameter and length of the plasma channel is 3mm and 60mm respectively. The discharge current was always 50A. Fig. 8 shows the results. The inlet pressure increases almost linearly from 20KPa to 60KPa with increasing the gas flow rate when the plasma window is on. And the pressure is much larger than that of plasma window off at the same gas flow rate. In other words, plasma window shows great effect on reducing gas consumption to maintain inlet pressure.

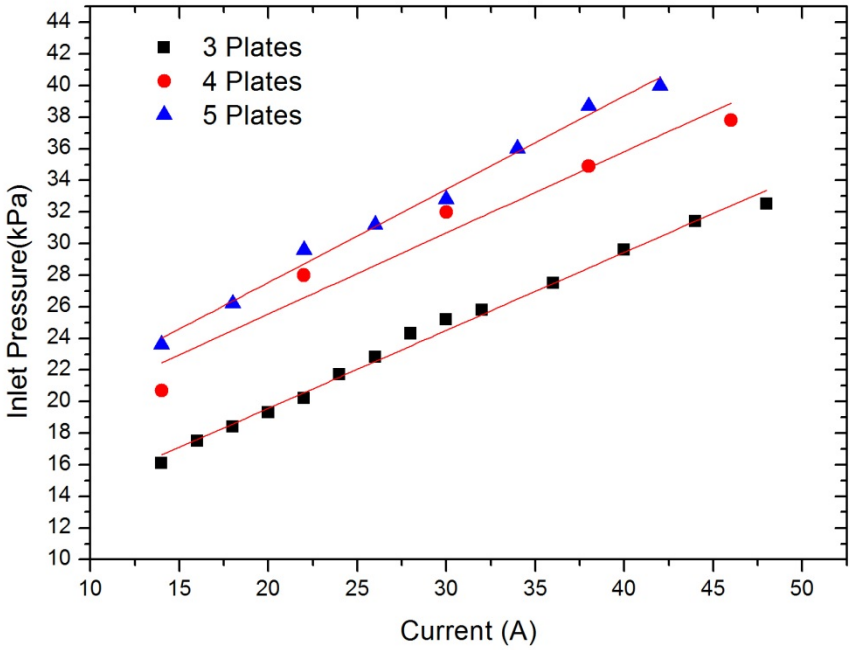

Figure 9: Pressure in experimental chamber as a function of current for channel length between 30 and 50mm. The channel diameter is 3mm.

Inlet pressure changing with arc current for channel length between 30 and 50mm was measured as shown in Fig. 9, from which we can find that the inlet pressure increases linearly with increasing the arc current. Besides, the length parameter of the plasma window shows a positive effect of increasing sealing ability. However such kind of effect is limited as length increases.

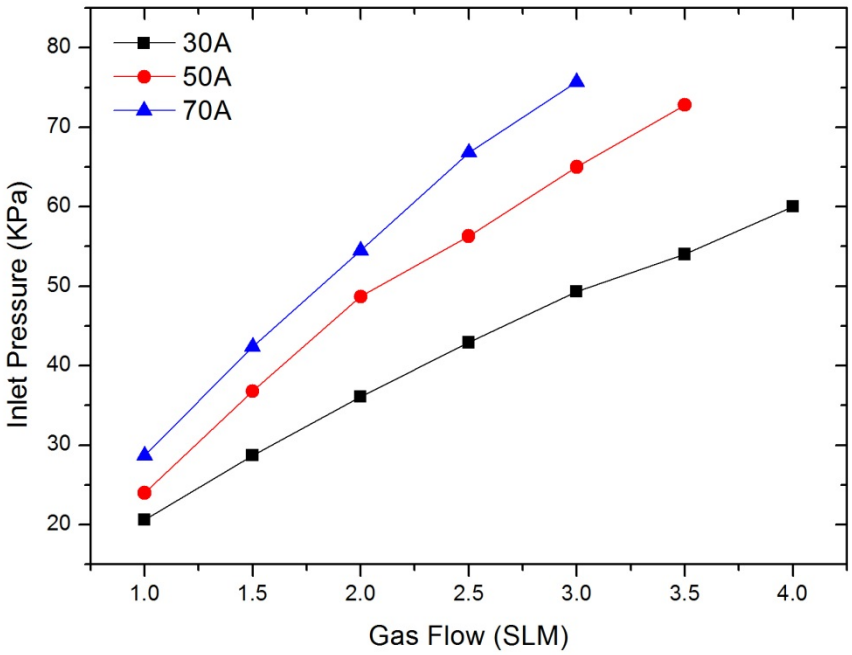

(a)

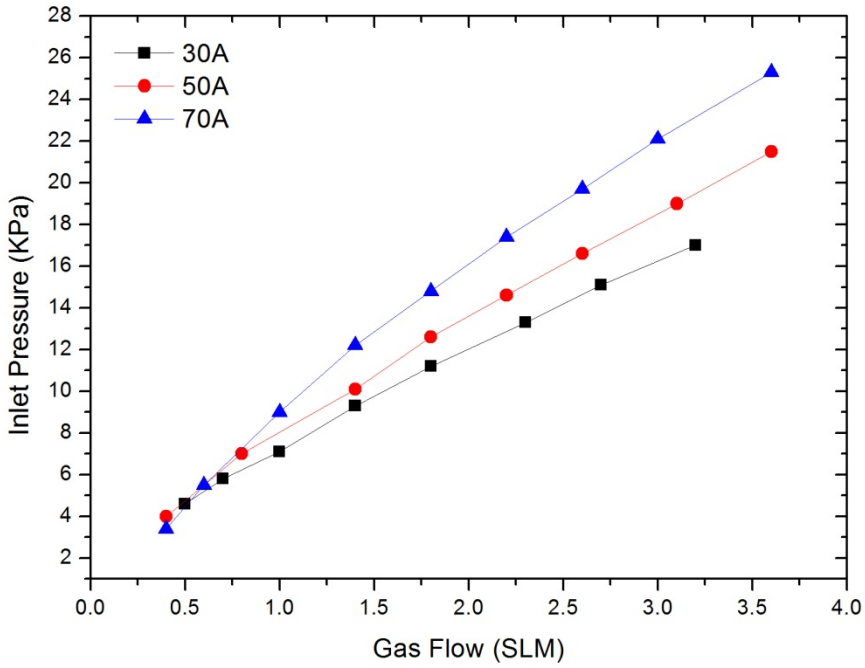

(b)

Figure 10: Pressure in experimental chamber in the function of gas flow rate for channel diameter of (a) 3mm and (b) 6mm at arc currents between 30A and 70A.

We also measured inlet pressure changes with gas flow for plasma channel diameters of

3mm and 6mm respectively. The results are shown in Fig. 10. By comparing figure10 (a) and 10 (b), we can find that diameter has a significant influence to sealing ability of plasma window. Inlet pressure drops drastically as the diameter increases when length, current and gas flow are specified.

As shown in Figures 9 and 10, inlet pressure is dependent on the total current, gas flow rate, discharge channel diameter and length. It is found that the plasma flow inside the arc channel is compatible with the description of a laminar flow from Ref. 19. Accordingly, in Fig. 11 we have normalized the inlet pressure to $\phi_{\text{gas flow rate}}^{0.5} d^{-2} l^{0.5}$ and plotted the result as a function of input power, which means there is no dependence of the normalized pressure on the channel diameter and length. The reason is that higher input power leads to the increase of sealing effectiveness, which can be ascribed to higher temperature and viscosity of plasma flow[17].

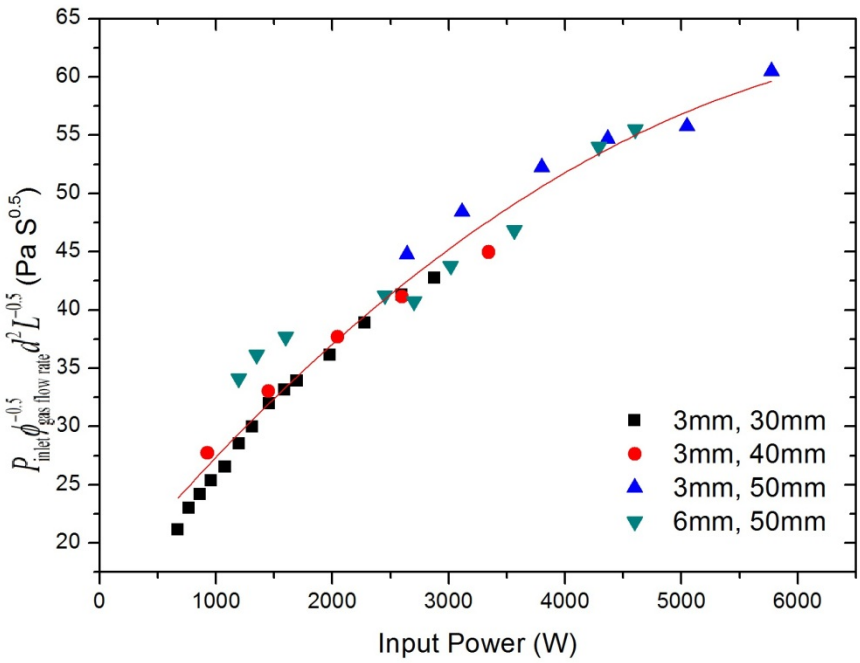

Figure 11: Inlet pressure normalized to the square root of gas flow rate, cross-sectional channel area and length as a function of input power for channel diameter 3mm, 6mm and length between 30mm and 50mm. For all measurements, the gas flow rate was 1.0SLM.

4. Comparison of experimental and simulation results and discussion

A. Viscosity and "thermal blocking" effect

The mechanisms of pressure gap within the plasma window can be attributed to two effects, which are viscosity effect and thermal-block effect according to reference [32]:
About 80% of pressure drop happens at the narrow cylindrical section of plasma window, which is mainly caused by viscosity effect and can be described by Poiseuille's equation[33] as follows

$$P_1 = \sqrt{P_2^{\,2} + \frac{256}{\pi}\eta_v \frac{l}{d^4}\frac{m}{M_0}RT}$$

Here P_1 and P_2 are the pressure at the inlet and the low pressure end of a tube, M_0 is the mole Moore molecular mass and η_v is the dynamic viscosity coefficient. The calculating results of the formula have a good agreement with the Fluent simulation. If $P_2 << P_1$, the equation can be rewritten as simple as

$$P_1 \approx 2.26\frac{\sqrt{\eta_v lNkT}}{d^2}.$$

The equation above clearly shows the relation between pressure drop with spatial structure parameters (discharge radius r and length l), and operating conditions (mass flow rate N and temperature T). One can see that viscosity effect of decreased discharge radius is far greater than the effect of increased length. Viscosity coefficient η_v increases almost linearly with temperature. For argon gas, the viscosity at 10000K is about 10 times bigger than at 300K. As a result, viscosity effect can also be enhanced by higher temperature.
The rest of pressure drop caused by thermal-block effect, which happens at stepped and divergent sections of plasma window, where viscosity effect becomes very small because of the large channel diameter. The pressure drop caused by thermal-block effect can be given by the equation[34]

$$p_1 - p_2 = \frac{\rho\overline{\Delta v}^2}{2}\eta_t$$

Where $\overline{\Delta v}$ is the average increase of flow speed caused by gas expansion in divergent sections and arc heating. η_t is called thermal-block coefficient, which is defined as coefficient of friction resistance. According to the above equation the large speed increase by heated gas expansion will lead to a steep pressure drop.

All measured sealing characteristics of plasma window described in section 4.C can be explained by these two pressure drop mechanisms. For discharge diameter, we can find that the increase of d will lead to decrease of temperature and also the viscosity. According to

equation, the viscosity effect will drop rapidly. On the other hand, we can expect the thermal block effect will also decrease as the eject efficiency will drop when increasing diameter. For discharge length, the viscosity effect will decrease gradually with decreasing length while the thermal-block effect is affected a little. Consequently, one can see that sealing pressure is far greater affected by decreasing diameter than the effect of increased length shown in figure 9 and figure 10. Increasing total current will mainly increase the temperature which will enhance the viscosity effect. At the same time, the increase of temperature will also help to increase η_t and average ejected flow speed. The thermal-block will be strengthened obviously. As a result, the sealing pressure will increase with increasing current as shown in figure 9.

B. Simulation results of MHD model

In order to validate the simulation model in reference 32, we compared the experimental data with the simulation results, including temperature, gas flow rate and total voltage changing with the current as shown in figure 10 . The simulation conditions are set as the same as experiment: a constant inlet pressure of 51 kPa is adopted; the discharge diameter and length are 3mm and 51mm respectively. The highest temperature along the axis of the model where the plasma is well developed was chosen to represent the temperature of simulation. It is comparable to the electron temperature detected by spectroscopy method. Figure 11a shows the result and we can find that the calculated results have a good agreement with the experimental data. However, the detected temperature is higher than the simulated temperature. This is partially because the LTE assumption is not valid in plasma window as discussed in section 3B; the electron temperature from spectroscopic measurements will be much higher than the heavy particle temperature. On the other hand, LTE assumption as well as neglect of radiation absorption in the simulation model will lead to a higher temperature gradient along radial direction, i.e. higher temperature near axis than experimental[35-37], which will decrease the difference between simulation and experiment temperature.

The calculated gas flow rate is compared with experiment in figure 11(b). The gas flow rate is mainly influenced by temperature distribution in the plasma window as other conditions are specified. From figure11b, we can find that the gas flow rate decreases while the temperature increases (please see figure11a) with changing the current. The calculated gas flow rate is in good agreement with experiment. The calculated total voltage is compared with experiment shown in figure 11(c). The slightly positive I-V characteristics from simulation results have a resonable agreement with experiment. However, the calculated voltage is higher than the experiment. This is partially because the LTE assumption leads to lower electrical conductivity than in the experiment. Besides, as the electrical conductivity decreases rapidly with radius, it will concentrate the heated plasma in the region near axis, the average radius of plasma of simulation will be larger than experiment. According to equation, these two factors will lead to a higher voltage of the simulation than the experiment.

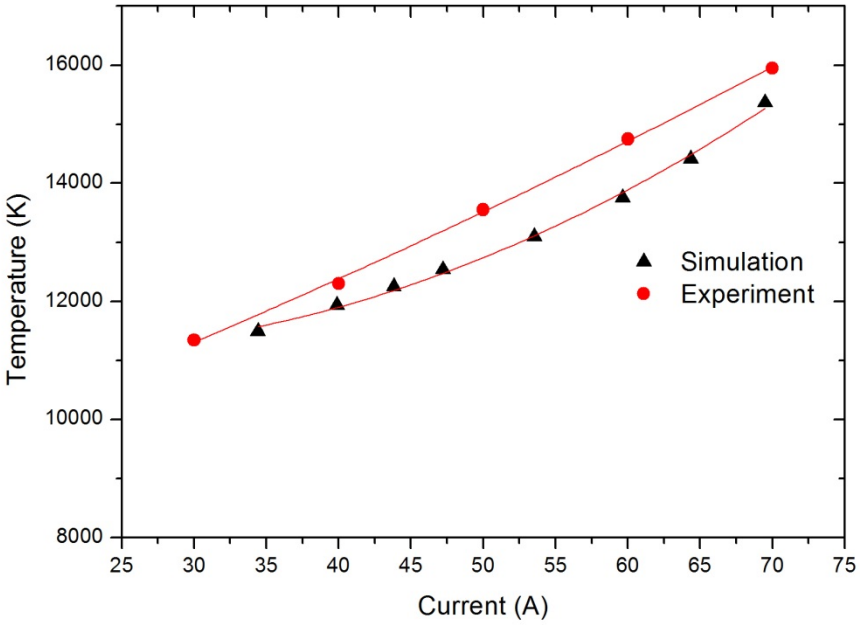
Temperature (K)
16000
14000
12000
10000
8000
25
30
35
40
45
50
55
60
65
70
75
Current (A)
Simulation
Experiment

(a)

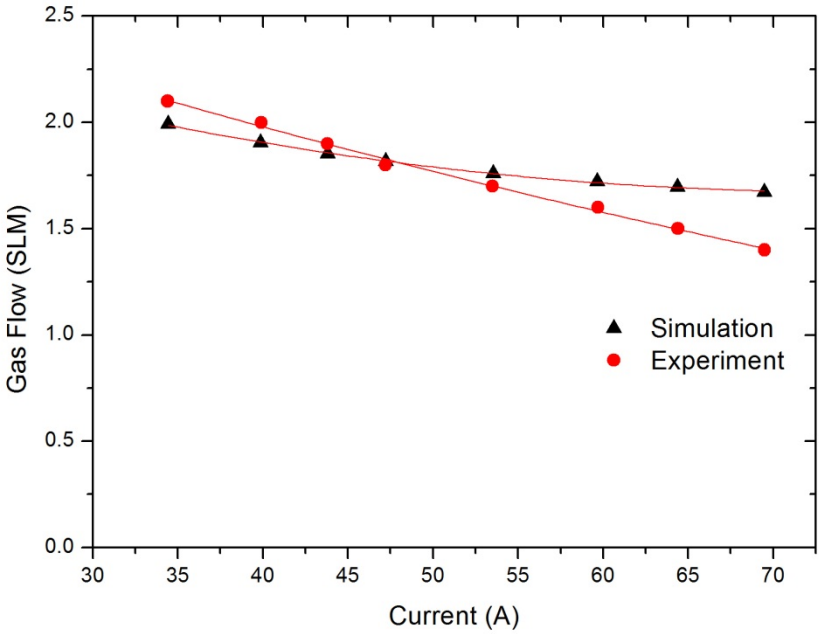
Gas Flow (SLM)
2.5
2.0
1.5
1.0
0.5
0.0
30
35
40
45
50
55
60
65
70
Current (A)
Simulation
Experiment

(b)

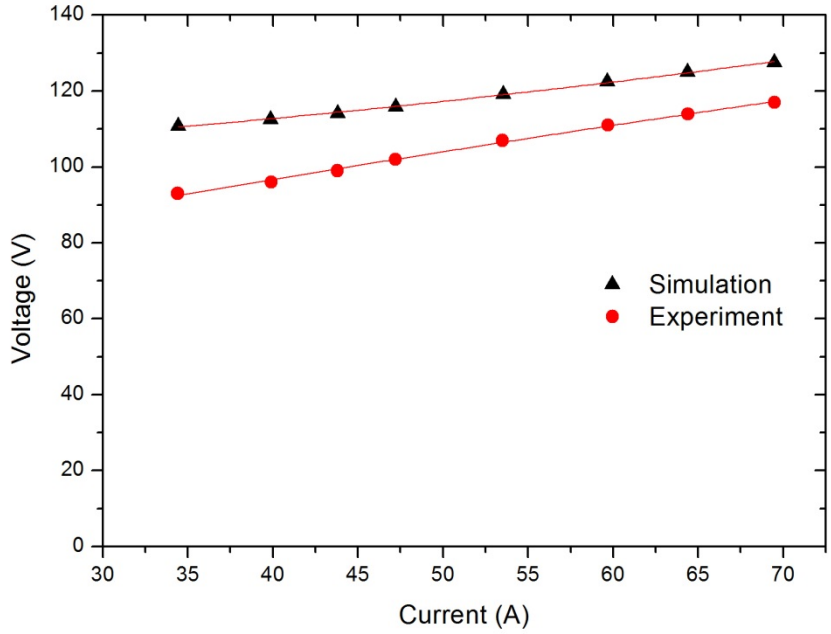

(c)

Figure 11: The (a) temperature, (b) gas flow rate and (c) total voltage changing with the current at given pressure of experimental chamber 51kPa. Discharge diameter and length are 3mm and 51mm respectively

It is shown that calculated results have a good agreement with the experimental data.

5. Conclusion

Plasma window with discharge channel diameters of 3 and 6mm and discharge length between 30 mm and 60 mm were experimentally investigated as a function of the operational parameters. Inlet pressure measurement shows that increasing discharge length will help to increase the sealing ability up to about 5 plates. But, when we use six cascaded copper plates, the improvement effect becomes comparatively small. On the other hand, discharge diameter plays a much more important factor on the influence of plasma window sealing ability than length. The inlet pressure increases almost linearly as increasing as gas flow and arc current. The measured I-V characteristic of plasma window is slightly positive which is quite different from other cascaded plasma devices. This phenomenon is caused by the radiation effect at lower discharge current. A spectroscopy setup was used to record the integrated spectral intensities emitted from the inlet side of plasma channel in the wavelength region of 410-550nm. The average electron temperature was estimated by atomic Boltzmann plot method. The variation of electron temperature due to arc current and gas flow was shown in this paper. By comparing the experimental results with those of simulation, the modeling seems to be validated. The 2D and

LTE MHD model predicts very reasonable voltage, temperature and gas flow results compared with the experiment. And the invalidation of LTE assumption employed in simulation model is the main factor for the differences between experiment and simulation results of temperature and voltage. To solve this problem, a two-temperature model[38-40] is usually suggested. Essentially, more comprehensive understanding of characteristic qualities of plasma window will be useful for more windowless sealing applications. And the simulation model will be reliable for optimization and innovation of plasma window design.

Acknowledgments

This work was supported by National Natural Science Foundation of China (Grant No.10805003 and No.91026012).

1. E. B. Iverson, R. C. Lanza and L. M. Lidsky, 1997 (unpublished).
2. A. de Beer, A. Hershcovitch, C. B. Franklyn, S. van Straaten and J. Guzek, Nuclear Instruments and Methods in Physics Research Section B: Beam Interactions with Materials and Atoms **170** (1–2), 259-265 (2000).
3. C. M. Jones, J. W. Johnson and R. M. Beckers, Nuclear Instruments and Methods **68** (1), 77-87 (1969).
4. W. Del Bianco and G. Kajrys, Nuclear Instruments and Methods in Physics Research **204** (2–3), 289-294 (1983).
5. U. Greife, C. Arpesella, C. A. Barnes, F. Bartolucci, E. Bellotti, C. Broggini, P. Corvisiero, G. Fiorentini, A. Fubini, G. Gervino, F. Gorris, C. Gustavino, M. Junker, R. W. Kavanagh, A. Lanza, G. Mezzorani, P. Prati, P. Quarati, W. S. Rodney, C. Rolfs, W. H. Schulte, H. P. Trautvetter and D. Zahnow, Nuclear Instruments and Methods in Physics Research Section A: Accelerators, Spectrometers, Detectors and Associated Equipment **350** (1–2), 327-337 (1994).
6. K. Sagara, A. Motoshima, T. Fujita, H. Akiyoshi and N. Nishimori, Nuclear Instruments and Methods in Physics Research Section A: Accelerators, Spectrometers, Detectors and Associated Equipment **378** (3), 392-398 (1996).
7. K. Sagara, S. Kamibeppu, H. Oba, H. Tanimoto, Y. Akama and M. Taniguchi, Nuclear Instruments and Methods in Physics Research Section A: Accelerators, Spectrometers, Detectors and Associated Equipment **590** (1-3), 194-197 (2008).
8. K. D. Bonin and T. J. McIlrath, Review of Scientific Instruments **55** (10), 1666-1668 (1984).
9. A. Hershcovitch, Journal of Applied Physics **78** (9), 5283-5288 (1995).
10. Y. P. Raizer, (New York: Springer-Verlag, 1991).
11. A. Hershcovitch, Physics of Plasmas **12** (5), 057102 (2005).
12. A. Hershcovitch, Nuclear Instruments and Methods in Physics Research Section B: Beam Interactions with Materials and Atoms **241** (1-4), 854-857 (2005).
13. A. Hershcovitch, Physics of Plasmas **15** (5), 057101 (2008).
14. B. T. Pinkoski, I. Zacharia, A. Hershcovitch, E. D. Johnson and D. P. Siddons, Review of Scientific Instruments **72** (3), 1677-1679 (2001).
15. H. Kuboki, H. Okuno, A. Hershcovitch, T. Dantsuka, H. Hasebe, K. Ikegami, H. Imao, O. Kamigaito, M. Kase, T. Maie, T. Nakagawa and Y. Yano, Journal of Radioanalytical and Nuclear Chemistry **299** (2),

1029-1034 (2014).
16. S. Huang, K. Zhu, B. L. Shi, Y. R. Lu, A. Hershcovitch, L. Yang, X. Y. Zhang and G. D. Wei, Physics of Plasmas (1994-present) **20** (7), - (2013).
17. Y. E. Krasik, S. Gleizer, V. Gurovich, I. Kronhaus, A. Hershcovitch, P. Nozar and C. Taliani, Journal of Applied Physics **101** (5), 053305 (2007).
18. W. A. J. Vijers, D. C. Schram, A. E. Shumack, N. J. L. Cardozo, J. Rapp and G. J. v. Rooij, Plasma Sources Sci. Technol **19**, 065016 (2010).
19. W. A. J. Vijers, C. A. J. v. Gils, W. J. Goedheer, H. J. v. d. Meiden, D. C. Schram, V. P. Veremiyenko, J. Westerhout, N. J. L. Cardozo and G. J. v. Rooij, Physics of Plasmas **15** (093507) (2008).
20. W. L. Wiese, J. W. Brault, K. Danzmann, V. Helbig and M. Kock, Physical Review A **39** (5), 2461-2471 (1989).
21. H. R. Greim, Cambridge University Press, 54-60 (1997).
22. N. K. Joshi, S. N. Sahasrabudhe, K. P. Sreekumar and N. Venkatramani, The European Physical Journal D - Atomic, Molecular, Optical and Plasma Physics **26** (2), 215-219 (2003).
23. J. J. Beulens, D. Milojevic, D. C. Schram and P. M. Vallinga, Phys. Fluids B **3** (9), 2548 (1991).
24. H. R. Griem, New York: McGraw-Hill (1964).
25. H. W. Drawin and P. Felenbok, Paris: Ganthier-villars (1965).
26. W. N. T. F. Kolesnikov, Inst. Akad. Nauk SSSR 33-66 (1964).
27. Bourasseau, D. Cabannes and F. Chapelle, J. Astr. Astrophys **9: 339** (1970).
28. A. Gleizes, H. Kafrouni, H. Duc and C. Maury, J. Phys. D: Appl. Phys **15**, 1031-1045 (1982).
29. D. C. Schram, S. Mazouffre, R. Engeln and M. C. M. v. d. Sanden, 209 (2001).
30. G. Zengyuan and Z. Wenhua, Science Press, Beijing (1986).
31. M. A. B and A. C. J, Plasma Chemistry and Plasma Processing **14:451-490** (1994).
32. S. Huang, K. Zhu, B. Shi and Y. Lu, Proceedings of IPAC2012, New Orleans, Louisiana, USA (2012).
33. B. E. Launder and D. B. Spalding, (Academic Press, London, England. 1972.).
34. G. Z. Yuan, B. W. Hong and Z. G. Zhong, Journal of Engineering Thermophysics **6** (N.2) (1985).
35. J. M. Bauchire, J. J. Gonzalez and A. Gleizes, Plasma Chemistry and Plasma Processing **17** (4), 409-432 (1997).
36. P. Freton, J. J. Gonzalez, A. Gleizes, F. C. Peyret, G. Caillibotte and M. Delzenne, Journal of Physics D: Applied Physics **35** (2), 115 (2002).
37. Q. Zhou, H. Li, X. Xu, F. Liu, S. Guo, X. Chang, W. Guo and P. Xu, Journal of Physics D: Applied Physics **42** (1), 015210 (2009).
38. K. S. C. Peerenboom, W. J. Goedheer, J. v. Dijk and J. J. A. M. v. d. Mullen, PLASMA SOURCES SCIENCE AND TECHNOLOGY **19** (2), 5009 (2010).
39. B. H. P. Broks, J. G. Keizer, R. A. B. Zijlmans and J. J. A. M. v. d. Mullen, Plasma Sources Science and Technology **15** (4), 865-872 (2006).
40. B. H. P. Broks, J. G. Keizer, R. A. B. Zijlmans, J. J. A. M. v. der and J. A. M. v. d. Mullen, PLASMA SOURCES SCIENCE AND TECHNOLOGY **15**, 865-872 (2006).